

Dimethyl fumarate protects against hepatic ischemia-reperfusion injury by alleviating ferroptosis via the NRF2/SLC7A11/HO-1 axis

Debin Qi*, Peng Chen*, Haili Bao, Lei Zhang, Keyan Sun, Shaohua Song, and Tao Li

Department of General Surgery, Ruijin Hospital, School of Medicine, Shanghai Jiao Tong University, Shanghai, China

ABSTRACT

Dimethyl fumarate (DMF), a therapeutic agent for relapsing-remitting multiple sclerosis, has cytoprotective and antioxidant effects. Ferroptosis, a pathological cell death process, is recently shown to play a vital part in ischemia-reperfusion injury (IRI). This study aimed to unveil the suppressive role of DMF on ferroptosis in liver IRI. The anti-ferroptosis effect of DMF on hepatic IRI was investigated using a liver IRI mouse model and a hypoxia-reoxygenation injury (HRI) model in alpha mouse liver (AML12) cells. Serum transaminase concentrations reflected liver function. Hematoxylin and eosin staining was used to assess liver damage. Cell viability was evaluated utilizing the CCK-8 assay. Malondialdehyde (MDA), the reduced glutathione/oxidized glutathione (GSH/GSSG) ratio, and BODIPY 581/591C11 were measured to estimate the injury caused by lipid peroxidation. Western blotting and real-time polymerase chain reaction (RT-PCR) were performed to explore the underlying molecular mechanisms. We demonstrated the anti-ferroptosis effects of DMF both in vivo and in vitro. DMF treatment ameliorated hepatic IRI. KEGG enrichment analysis and transmission electron microscopy revealed a close relationship between ferroptosis and liver IRI. Furthermore, DMF protected against HRI by inhibiting ferroptosis via activating the nuclear factor E2-related factor 2 (NRF2) pathway. Interestingly, NRF2 knockdown notably decreased the expression of SLC7A11 and HO-1 and blocked the anti-ferroptosis effects of DMF. DMF inhibits ferroptosis by activating the NRF2/SLC7A11/HO-1 axis and exerts a protective effect against hepatic IRI.

ARTICLE HISTORY

Received 19 September 2022
Revised 17 November 2022
Accepted 1 December 2022

KEYWORDS

Dimethyl fumarate;
ischemia-reperfusion injury;
ferroptosis; NRF2; SLC7A11

1. Introduction

Ischemic tissues and organs suffer aggravated tissue damage after blood perfusion, termed ischemia-reperfusion injury (IRI). The normal functional metabolism of the liver is highly dependent on oxygen supply, and IRI is inevitable in liver transplantation, hemorrhagic shock, and severe trauma [1]. Therefore, inhibiting liver IRI would improve clinical outcomes and expand the donor pool by utilizing marginal liver grafts [2]. Despite its clinical importance, the mechanisms underlying liver IRI remain unclear, and effective preventive and therapeutic strategies are required. IRI is closely related to an increase in free radical generation, among which $\text{OH}\cdot$ is the most active oxygen free radical. The increase in ferrous iron ions or copper ions accelerates the reaction rate of H_2O_2 to $\cdot\text{OH}$, which is called the Fenton/Haber-Weiss reaction [3].

Ferroptosis, a distinct iron-dependent cell death paradigm, causes cell death via extensive lipid peroxidation [4]. It plays a necessary part in oxidative stress-related diseases, including tumors, nervous system diseases, and acute kidney injury [5]. Inhibition of ferroptosis has been demonstrated in recent research to be a viable therapeutic method for heart, kidney, and lung IRI, while ferroptosis inducers can be optimized as antitumor agents [6–9]. However, there is limited evidence of ferroptosis in liver IRI and a lack of a defined treatment strategy.

Dimethyl fumarate (DMF), a derivative of the Krebs cycle intermediate fumarate, has been confirmed with cytoprotective and antioxidant effects that activate the nuclear factor E2-related factor 2 (NRF2) pathway [10,11]. In chronic cerebral hypoperfusion, alcoholic liver disease, acute kidney injury and acute lung injury models, DMF

CONTACT Keyan Sun  188025796@qq.com; Shaohua Song  77472087@163.com; Tao Li  transplant@126.com  Department of General Surgery, Ruijin Hospital, School of Medicine, Shanghai Jiao Tong University, No.197, Ruijin 2nd Road, Huangpu District, Shanghai, 200025, China

*These 2 authors have equally contributed.

© 2022 The Author(s). Published by Informa UK Limited, trading as Taylor & Francis Group.

This is an Open Access article distributed under the terms of the Creative Commons Attribution-NonCommercial-NoDerivatives License (<http://creativecommons.org/licenses/by-nc-nd/4.0/>), which permits non-commercial re-use, distribution, and reproduction in any medium, provided the original work is properly cited, and is not altered, transformed, or built upon in any way.

inhibited ferroptosis through the NRF2 signaling pathway, showing a significant protective effect [12–15]. NRF2 is an anti-ferroptosis transcriptional regulator that can prevent the accumulation of free iron and lipid peroxidation [16]. Multiple human malignancies have elevated levels of the cystine/glutamate antiporter SLC7A11, which imports cystine for glutathione production and antioxidant defense. According to recent research, SLC7A11 overexpression encourages tumor development in part by inhibiting ferroptosis [17] and NRF2 reduces ferroptosis via modulating SLC7A11 and HO-1 [18].

This research focused on seeing how DMF affected ferroptosis in liver IRI. We found that DMF attenuated IRI-induced liver damage, inflammation, and ferroptosis in an IRI mouse model and explored the underlying molecular mechanisms in an HR cell model. And we confirmed that DMF inhibited ferroptosis by activating the NRF2/SLC7A11/HO-1 axis. Our research sheds new light on the mechanism of DMF in ferroptosis and identifies a previously untapped therapeutic target for liver IRI.

2. Materials and methods

2.1. Animals and hepatic IR surgery

Joint Ventures Sipper BK Experimental Animals (Shanghai, China) provided eight to ten-week-old male C57BL/6J mice (20–25 g body weight). All animals in this study were bred in a conventional SPF animal room with a 12:12-hour light/dark cycle and free access to food and water. The Shanghai Jiao Tong University School of Medicine's Institutional Animal Care and Use Committee (Shanghai, China) examined and authorized all animal procedures and provide the ethical clearance statement (SYXK-2018-0027).

DMF (242926; Sigma-Aldrich, St. Louis, MO, USA) was dissolved in dimethyl sulfoxide (DMSO) (vehicle). The mice were randomly divided into four groups of six: sham+ vehicle, sham+ DMF, IR+ vehicle, and IR+ DMF. The mice were supplemented with DMF at a concentration of 100 mg/kg or DMSO by daily

oral gavage for a week before surgery, as previously reported [10].

As stated in a prior study, the partial warm liver IRI model was developed [19]. Briefly, the sham group only had free hepatic portal blood vessels after laparotomy, and the blood flow was not obstructed. As for the hepatic IR group, the blood supply to the left and mid-hepatic lobes was blocked, resulting in 70% mouse liver IRI for 90 min. The mice were put on a heated blanket after surgery in order to maintain body temperature and monitor vital signs. Blood supply was restored for 6 h. Died mice were eliminated for testing prior to sample collection. The mice were euthanized after the sample were obtained. The same experimenter carried out all surgeries.

2.2. Assessment of liver function

After reperfusion, serum aspartate transaminase (AST) and alanine transaminase (ALT) concentrations were measured using a standard modular auto-analyzer (NX500i, FUJIFILM, Japan) according to the manufacturer's procedure.

2.3. Histopathological examination

For staining, tissue samples were fixed overnight in 4% paraformaldehyde, embedded in paraffin wax, and serially sectioned at 4 μ m thickness. At least 10 high-power fields (magnifications of 10 \times and 40 \times) per slice were evaluated for each tissue sample. Histopathological damage was assessed using Suzuki's histological grading system [20].

2.4. Real-time (RT)-PCR analysis

Total RNA was extracted from liver tissue and AML12 (alpha mouse liver 12) cells using a TRIzol reagent kit (Invitrogen, Waltham, MA, USA) and reverse-transcribed into first-strand cDNA using HiScript III-RT SuperMix (+gDNA wiper; Vazyme Biotech, China) for quantitative polymerase chain reaction (qPCR). AceQ Universal SYBR qPCR Master Mix (Vazyme Biotech) was used to quantify relative RNA expression levels determined by reverse transcription-qPCR (RT-qPCR) on a 384-well plate. The levels of relative expression were compared to those of β -

Gene	Forward (5' to 3')	Reverse (5' to 3')
IL1 β	ATGAAGGGCTGCTCCAAAC	TCTCCACAGCCACAATGAGT
IL6	GGAGCCACCAAGAACGATA	ACCAGCATCAGTCCCAAGAA
TNF α	CTCATGCACCACCATCAAGG	ACCTGACCACTCTCCCTTTG
β -actin	AACAGTCCGCCTAGAAGCAC	CGTTGACATCCGTAAGACC
GPX4	TGTGCATCCCGCATGATT	CCCTGTACTIONTCCAGGAGAA
COX2	ATTCTTTGCCAGCACTTC	GATACACCTCTCCACCAATGA
NRF2	AGTGACTCGAAATGGAGGAG	TGTGCTGGCTGTGCTTTAGG
SLC7A11	GCTGACACTCGTCTATT	ATTCTGGAGGTCTTTGGT
HO-1	GATAGAGCGCAACAAGCAGAA	CAGTGAGGCCCATACCAGAA

actin. The following were the primer sequences used:

2.5. Immunofluorescence staining

Liver tissues were air-dried, fixed with acetone at -20°C , then treated with a primary antibody against F4/80 (GB11027, Servicebio<Wuhan, China) and MPO (GB11224, Servicebio, Wuhan, China) overnight at 4°C to inhibit nonspecific binding. The liver slices were washed and immunostained with secondary antibodies for 1 hour at 37°C . DAPI was used to stain the sections' nuclei. Images were obtained using a fluorescence microscope (DX51; Olympus) and quantified using Image-Pro Plus software.

2.6. RNA Sequencing

The liver tissues of sham or IR operated mice ($n = 3$ in each group) were used for RNA sequencing (RNA-seq). RNA isolation, library construction, and sequencing were performed by BGI using a BGISEQ-500 RNA-seq platform (Beijing Genomic Institution, www.genomics.org.cn, BGI). KEGG enrichment analyses were implemented by the KOBAS2.0 software (<http://kobas.cbi.pku.edu.cn>). The KEGG pathways with P value <0.05 were considered as enriched.

2.7. Transmission electron microscopy (TEM)

1.25% glutaraldehyde/0.1 M phosphate buffer was used to fix liver tissues, which were then postfixed in 1% OsO₄/0.1 M phosphate buffer. A microtome was used to cut ultrathin slices (50 nm), which were then put on copper grids and stained with

uranyl acetate and lead citrate before being studied under an electron microscope (HT7800, HITACHI, Tokyo, Japan). To quantify mitochondrial damage, five random visual fields from each sample were evaluated.

2.8. Measurement of malondialdehyde (MDA), reduced glutathione (GSH), and oxidized glutathione disulfide (GSSG)

According to the manufacturer's instructions, the levels of MDA in liver tissues and AML12 cells were detected using a lipid peroxidation MDA assay kit (S0131; Beyotime, Shanghai, China). GSH and GSSG levels in liver tissues and AML12 cells were measured using a commercially available GSH and GSSG assay kit (RK05819; ABclonal Technology, Woburn, MA, USA).

2.9. Immunohistochemistry (IHC) staining

Primary NRF2 antibody (Proteintech; 16396-1-AP, 1:50) was incubated with the liver slices overnight at 4°C . Then, the sections were incubated with horseradish peroxidase-conjugated secondary antibody for 60 min at RT after washing with TBST buffer three times. Finally, the peroxidase conjugates were stained with a DAB kit (ZLI-9018, Zsbio, China), and the images were captured using an Olympus B \times 51 microscope (Olympus, Center Valley, PA).

2.10. Western blotting

Target proteins in liver samples and cell extracts were quantified using Western blotting. In a nutshell, 40 μg of total protein from each sample

was utilized for western blot analysis, which was carried out using a standard methodology. The following antibodies were used: β -actin (66009-1-Ig; 1:1000; ProteinTech Group, Chicago, IL, USA), GPX4 (59735; 1:1000; Cell Signaling Technology), COX2 (12282; 1:1000; Cell Signaling Technology), NRF2 (16396-1-AP; 1:800; ProteinTech Group), SLC7A11 (26864-1-AP; 1:1000; ProteinTech Group), and HO-1 (86806; 1:1000; Cell Signaling Technology). The Tanon-5200 Chemiluminescent Imaging System was used to collect the data, and ImageJ (NIH, Bethesda, MD, USA) was used to perform densitometric analysis of the immunoblotting bands.

2.11. Cell culture and hypoxia-reoxygenation (HR) model

The manufacturer's guidelines were followed for maintaining the mouse hepatic cell line AML12 (ATCC, Manassas, VA, USA). To establish the HR model, AML12 cells were washed with PBS, and the medium was replaced with DMEM/F12 medium without glucose or serum. The cells were placed in a tri-gas incubator (Smartor 118pro) with a hypoxic gas mixture (5% CO₂, 94% N₂, and 1% O₂) at 37°C for 12 h. Then the cells were placed in a 5% CO₂ incubator with a complete medium for 12 h. Monomethyl fumarate (MMF; S6889; Selleck Chemicals, Houston, TX, USA), Liproxstatin-1 (100 nM, MCE, HY-12726) and Z-VAD-FMK (20 μ m, Adooq BioScience, Irvine, CA) were added 1 h before the HR stimulation.

2.12. Detection of cell viability

The cell viability was determined using a CCK-8 assay kit (MA0218-L; Meilun Biotechnology, Dalian, China). A microplate reader was used to measure absorbance at 450 nm (BioTek, Winooski, VT, USA).

2.13. BODIPY 581/591 C11 staining

Lipid peroxidation level was assessed using BODIPY 581/591 C11 staining (RM02821; ABclonal). The stained cells were analyzed by flow cytometry using CytoFLEX5 (Beckman Coulter) and an LSM 710 confocal microscope (Carl Zeiss).

2.14. Small interfering RNA transfection

Shanghai Bioegene Co., Ltd (China) generated both NRF2 and negative control small interfering RNAs (siRNAs). Before transfection, AML12 cells were seeded in plates and cultured over 24 hours. When attaining 70–90% confluence, the cells were transfected with HilyMax (H357; Mojindo Molecular Technologies, Inc., Rockville, MD, USA).

2.15. Statistical analyses

GraphPad Prism 9 (San Diego, CA, USA) was used for all data analysis. The data was given in the form of a mean and standard deviation (SD). An unpaired Student's t-test or analysis of variance (ANOVA) was used for statistical analysis. $P < 0.05$ was chosen as the threshold for statistical significance.

3. Results

3.1. DMF treatment ameliorates liver IRI in mice

To investigate the functional role of DMF in hepatic IRI, mice were randomly divided into four groups of six: sham+ vehicle, sham+ DMF, IR+ vehicle, and IR + DMF. DMF-treated groups were administered with an intraperitoneal injection of DMF, as previously reported [19], whereas the vehicle group mice were treated with the same dose of DMSO. Notably, compared with the IR group, DMF protected against IRI, as demonstrated by a marked decrease in ALT and AST levels (Figure 1(a)). The Suzuki scores of the groups varied substantially, indicating that DMF pretreatment ameliorated IRI and induced histological changes (Figure 1(b) and 1(c)). In addition, immunohistochemical labeling of F4/80 and MPO was performed to assess inflammatory infiltration (Figure 1(d) and 1(e)). Significantly high levels of the inflammatory cytokines IL-1, IL-6, and TNF in the livers of the IR group were verified by RT-PCR, which was dramatically reduced by DMF treatment (Figure 1(f)).

3.2. DMF reduces ferroptosis in liver IRI

We had previously shown that DMF improved liver IRI, but it was unknown if DMF could

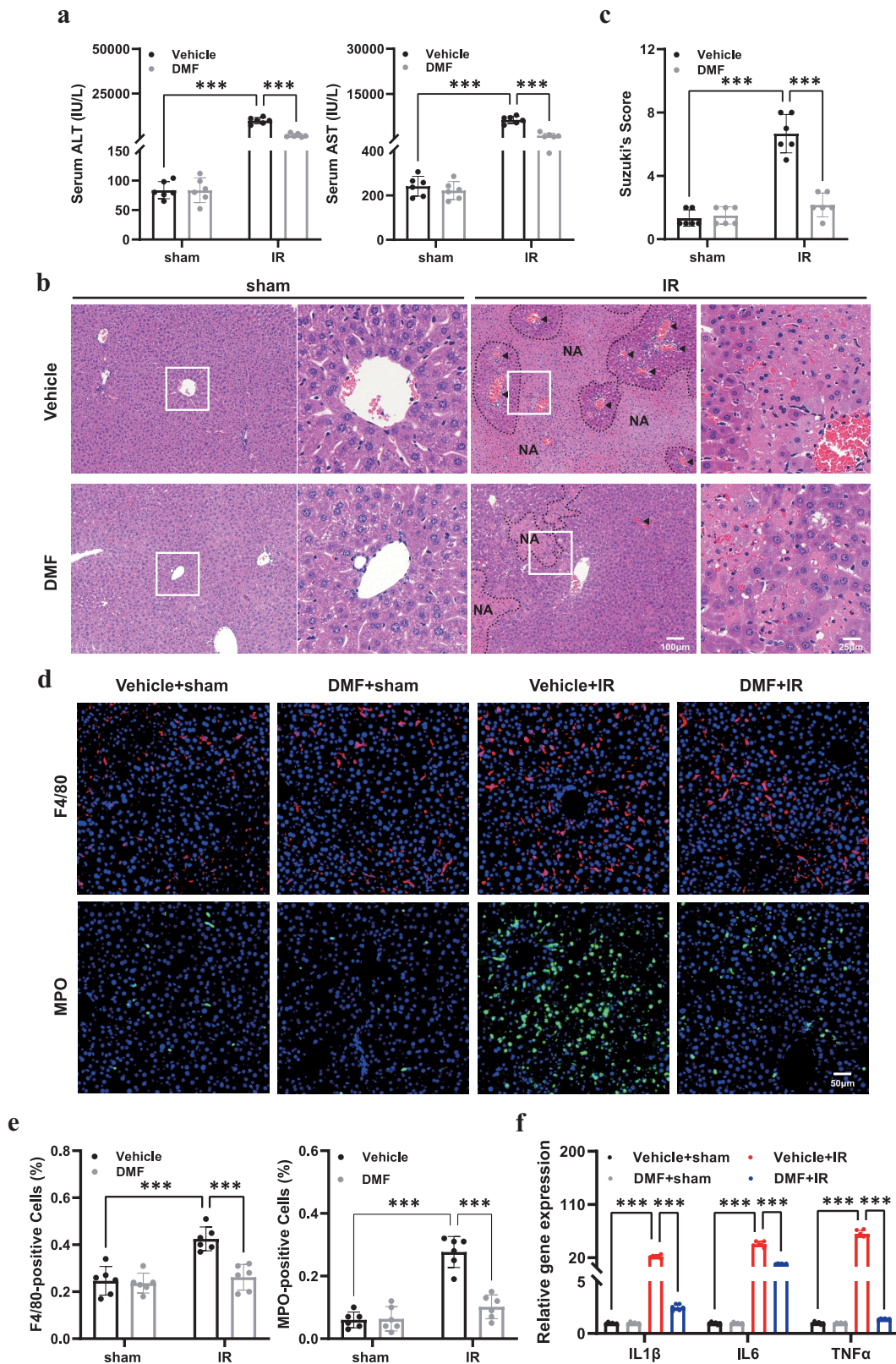


Figure 1. DMF treatment ameliorates IRI in mice. (a) Serum aspartate transaminase (AST) and alanine transaminase (ALT) of vehicle- or DMF-treated mice were measured after sham or IR procedure. (b) Representative hematoxylin and eosin (H&E) staining of liver tissues in different groups. Necrotic areas were marked with "NA" and vascular congestion with arrows. (n = 6, original magnification, $\times 10$ and $\times 40$, Scale bar, 100 μm , 25 μm). (c) Quantitative assessment of the levels of liver damage using Suzuki's histological criterion. (d, e) Representative F4/80 and MPO staining of liver sections to assess inflammatory infiltration after IR with the administration of DMF. (n = 6, original magnification, $\times 20$, Scale bar, 50 μm). (f) the mRNA expression of inflammatory cytokines. The results are shown as mean \pm SD of six mice in each group. *** $P < 0.001$, ** $P < 0.01$, * $P < 0.05$ (analyzed by one-way analysis of variance, ANOVA).

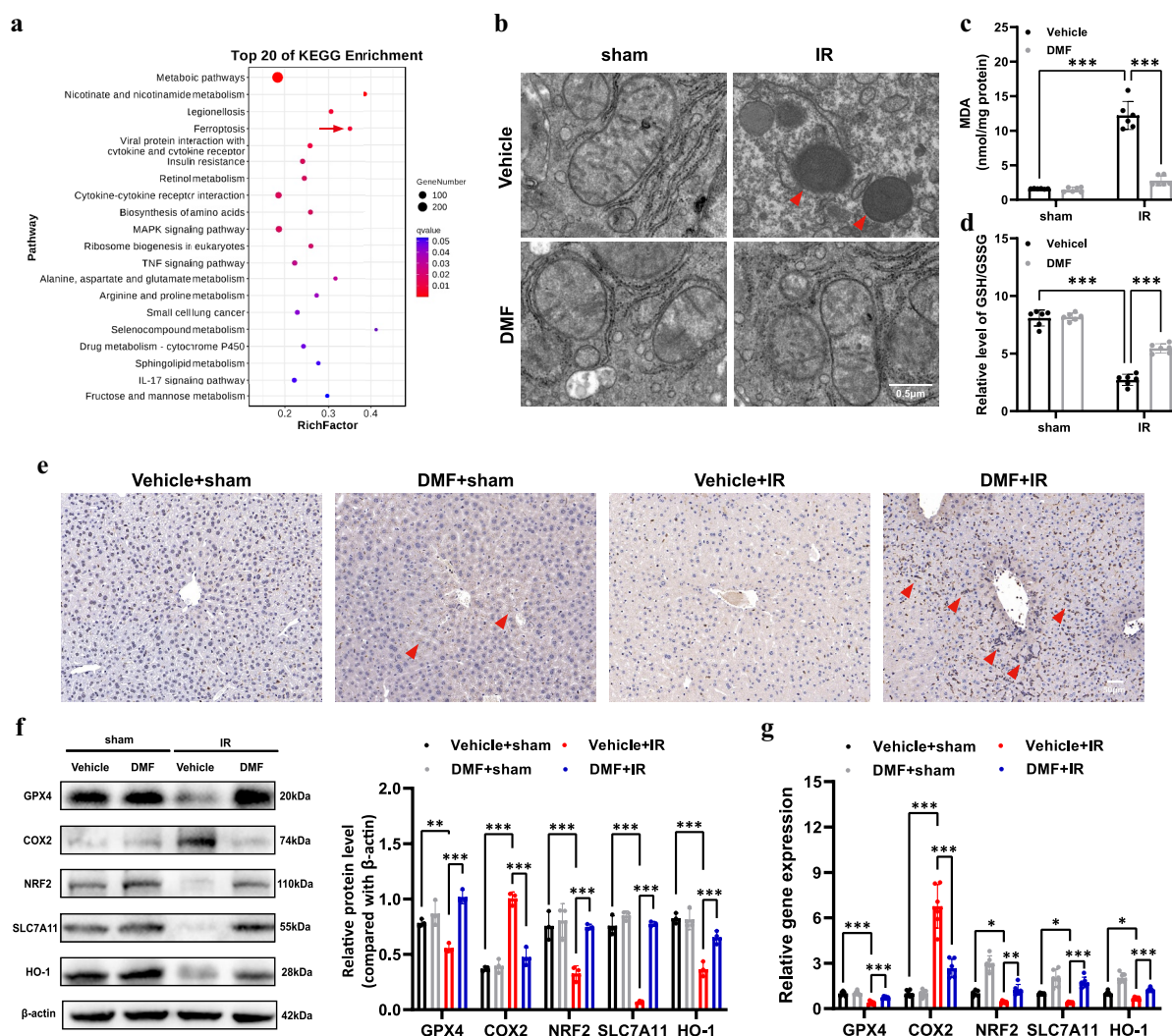


Figure 2. DMF reduces ferroptosis in IRI. (a) KEGG pathway classification and enrichment of differentially expressed genes in the sham versus IR groups. (b) Representative transmission electron microscopy images of mitochondria in hepatocytes of the liver. Red arrow: damaged mitochondria. (c) the level of lipid peroxide malondialdehyde (MDA) in each group. (d) the relative GSH/GSSG ratio in the liver of mice. (e) Representative immunohistochemistry (IHC) staining of NRF2 in the liver of each group, and NRF2 positive areas were marked with arrows. (n = 6, original magnification, $\times 20$, Scale bar, 50 μm). (f) Western blot and quantification of hepatic GPX4, COX2, NRF2, SLC7A11, and HO-1 proteins. (g) Relative mRNA expression of GPX4, COX2, NRF2, SLC7A11, and HO-1 in each group. The results are shown as mean \pm SD of six mice in each group. *** $P < 0.001$, ** $P < 0.01$, * $P < 0.05$ (analyzed by one-way analysis of variance, ANOVA).

alleviate liver IRI by relieving ferroptosis. The KEGG pathway enrichment analysis results showed that ferroptosis was the main differentially expressed pathway in the sham versus IR groups (Figure 2(a)). Electron microscopy studies of liver tissues in the IR group revealed shrunken mitochondria with increased membrane density, whereas those of the DMF-treated group didn't show the change in mitochondrial morphology (Figure 2(b)). We then estimated lipid peroxidation levels, a hallmark of ferroptosis, using an MDA assay (Figure 2(c)) and the GSH/GSSG

ratio (Figure 2(d)). Interestingly, the IR group showed increased lipid peroxidation, which was alleviated by DMF treatment. The protein levels of the NRF2 were efficiently increased after DMF treatment (Figure 2(e)). As shown in Figure 2(f), hepatic GPX4, NRF2, SLC7A11, and HO-1 expression decreased after IRI; however, this decrease in expression was remarkably rescued by DMF treatment. In addition, western blot analysis showed that IR induced an increase in COX2 expression, one of the most upregulated proteins in ferroptosis, which was inhibited by DMF treatment. The

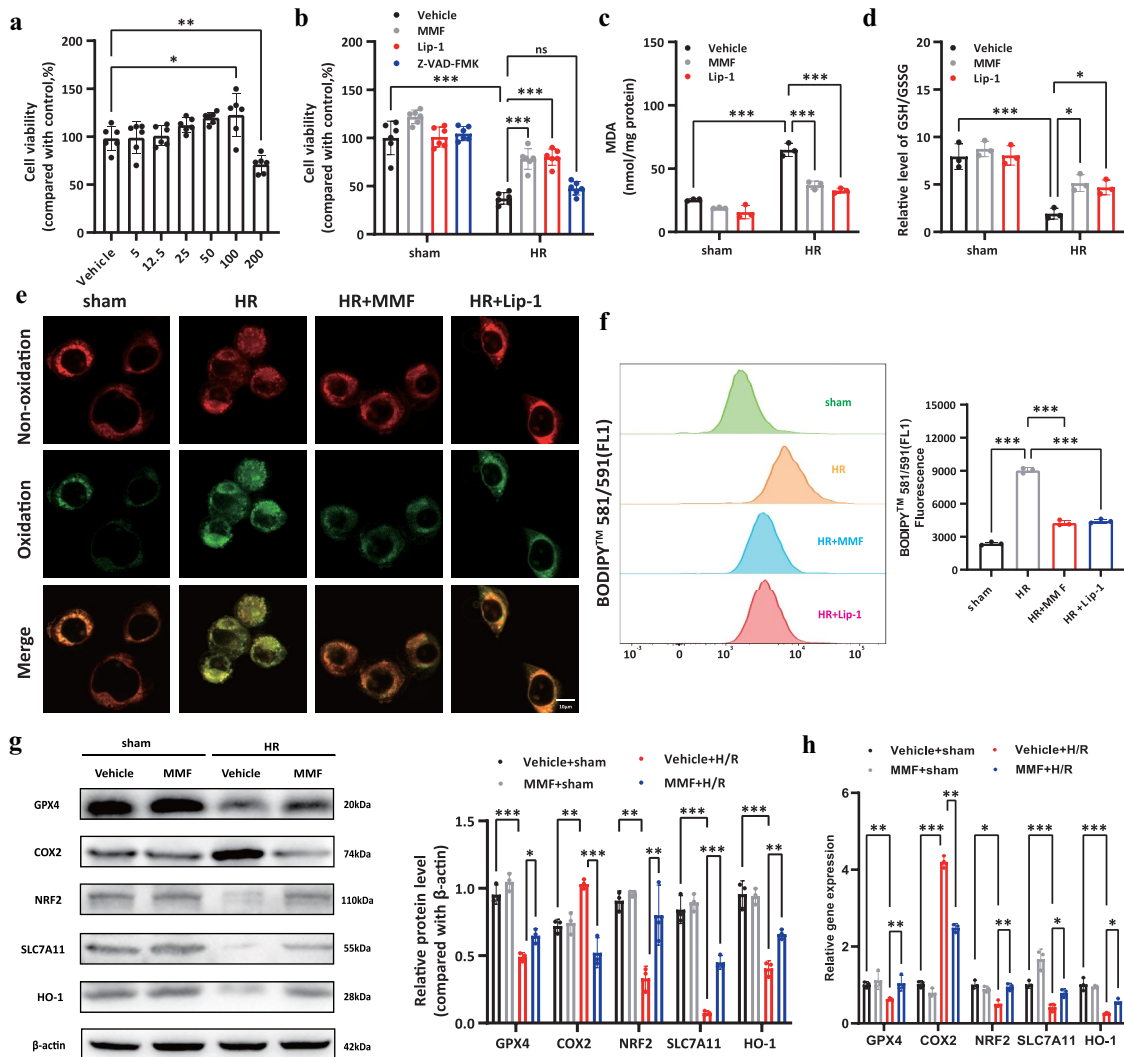


Figure 3. MMF attenuates ferroptosis in AML12 cells during hypoxia-reoxygenation injury (HRI). (a) CCK-8 assay showed the viability of AML12 cells after treatment with various MMF concentrations (5 μM–200 μM) for 24 h. (b) Cell viability of AML12 cells with HRI treated with MMF (100 μM), Lip-1 (100 nM) or Z-VAD-FMK (20 μM) for 1 h. (c, d) the levels of MDA and GSH/GSSG ratio in each group. (e, f) C11-BODIPY581/591 was used to monitor the oxidized and nonoxidized variants of lipid peroxides, observed by confocal microscopy and flow cytometry. (g, h) Western blotting and RT-PCR revealed the changes in the expression levels of GPX4, COX2, NRF2, SLC7A11, and HO-1 in AML12 cells. The results are shown as mean ± SD. *** $P < 0.001$, ** $P < 0.01$, * $P < 0.05$ (analyzed by one-way analysis of variance, ANOVA).

RT-PCR results matched the western blotting results (Figure 2(g)).

3.3. MMF attenuates ferroptosis in AML12 cells after HRI

In AML12 cells, the effects of DMF were tested with or without hypoxia for 12 hours and reoxygenation for 12 hours. In vivo, DMF is rapidly converted to MMF. Hence MMF was employed in cell culture tests. The CCK-8 test was utilized to measure the MMF concentration in this investigation, which was 100

μM. (Figure 3(a)). The results of the CCK-8 assay (Figure 3(b)) demonstrated that MMF treatment reduced HRI-induced AML12 cell death. Liproxtatin-1 (Lip-1), an effective inhibitor of ferroptosis, was used as the positive control. However, Z-VAD-FMK (a kind of apoptosis inhibitor) didn't show protective effect. MMF prevented the lipid peroxidation produced by HRI, according to the results. (Figure 3c–f). In addition, western blot analysis and RT-PCR results for GPX4, COX2, NRF2, SLC7A11, and HO-1 confirmed the protective role of MMF in ferroptosis during HRI (Figure 3g and 3h).

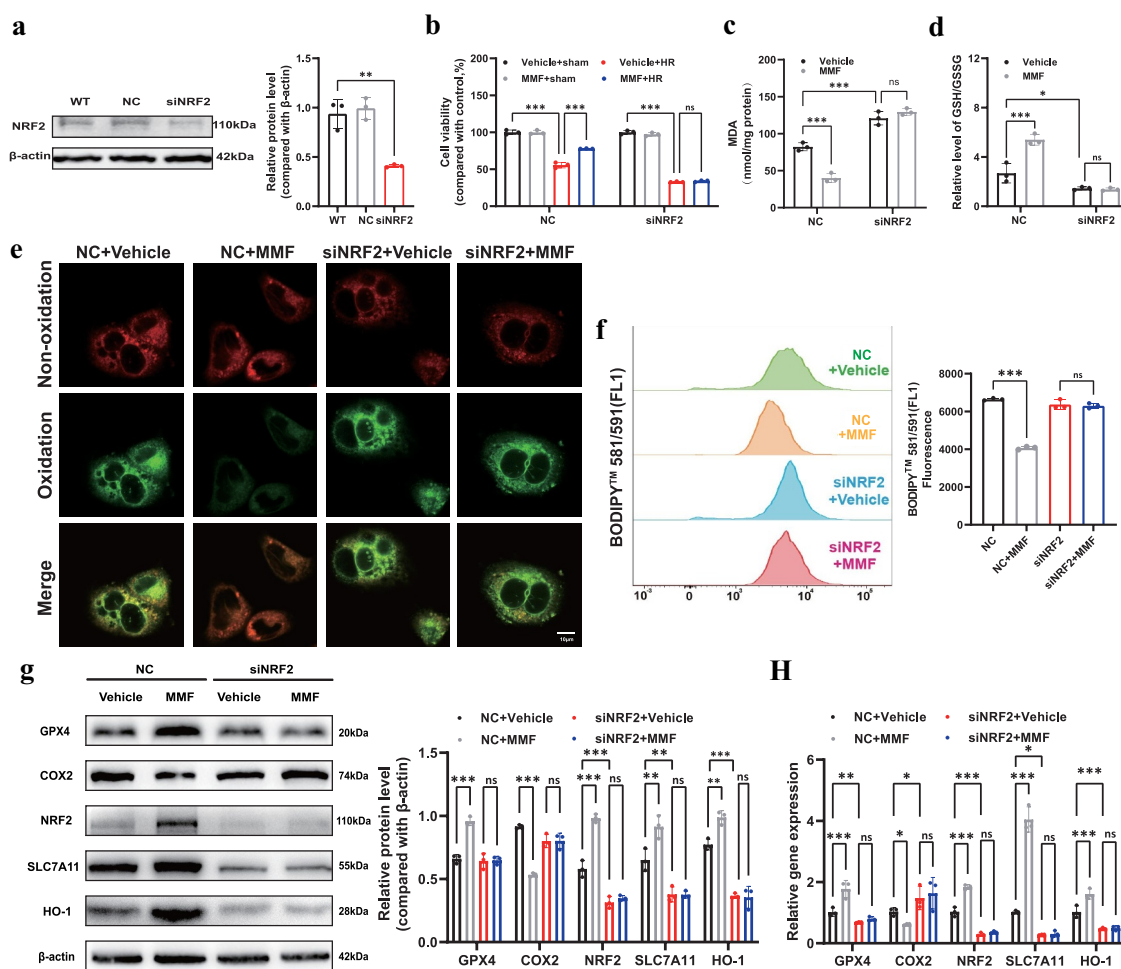


Figure 4. MMF alleviates ferroptosis via the NRF2/SLC7A11/HO-1 axis. AML12 cells were transfected with siRNA against NRF2 under hypoxia for 12 h and reoxygenation for 12 h. (a) NRF2 knockdown by siRNA in AML12 cells was confirmed by western blot analysis. (b) CCK-8 assay showing hypoxia-reoxygenation injury (HRI)-induced NC- or siNRF2- AML12 cell death with or without MMF. (c-f) MDA, the GSH/GSSG ratio, and BODIPY 581/591C11 were detected in each group. (g, h) Western blotting and RT-PCR showed the changes in expression of GPX4, COX2, NRF2, SLC7A11, and HO-1 in AML12 cells. The results are shown as mean \pm SD. *** $P < 0.001$, ** $P < 0.01$, * $P < 0.05$, ns: no significance (analyzed by two-way analysis of variance ANOVA).

3.4. MMF alleviates ferroptosis via the NRF2/SLC7A11/HO-1 axis

Small interfering RNAs (siRNAs) were used to downregulate NRF2 expression in cultured AML12 cells to see if it mediated the protective effect of DMF. (Figure 4(a)). NRF2 downregulation significantly deteriorated HRI, which was not alleviated by MMF treatment (Figure 4(b)). The siNRF2 group had higher MDA levels and GSH/GSSG ratios compared to the NC group, which greatly reduced the protective effects of MMF (Figure 4(c) and 4(d)). As shown in Figure 4(e) and 4(f), the BODIPY 581/591C11 probe revealed that the lipid peroxidation level in the siNRF2 group was not reversed by MMF treatment. After

inducing HRI, the siNRF2 + vehicle group showed remarkably inhibited expression of SLC7A11 and HO-1 compared with the NC + vehicle group. However, there was no statistical difference between the siNRF2+ vehicle and siNRF2 + MMF groups (Figure 4(g)). The RT-PCR findings (Figure 4(h)) matched the western blotting results.

4. Discussion

The present study demonstrated the anti-ferroptosis role of DMF in hepatic IRI. We revealed that DMF attenuated IRI-induced liver damage, inflammation, and ferroptosis in an IRI mouse model and explored the underlying

molecular mechanisms in an HR cell model. DMF is a prodrug that is rapidly converted to MMF in the body after oral ingestion. We revealed that MMF inhibited lipid peroxidation and ferroptosis in AML12 cells after HR injury and upregulated the expression of NRF2, SLC7A11, and HO-1. In addition, NRF2 downregulation by siRNA reversed the protective role of MMF and decreased the expression of SLC7A11 and HO-1. In summary, we confirmed that DMF inhibited ferroptosis by activating the NRF2/SLC7A11/HO-1 axis and exerted a protective effect against hepatic IRI.

Ferroptosis is a one-of-a-kind mode of cell death, that brings iron, selenium, redox chemistry, lipids, and amino acids together into a cohesive network. However, the mechanisms that regulate ferroptosis and cell death deserve further study. Ferroptosis is strongly suggested as a significant contributor to cell death associated with IRI, especially in ischemic heart disease, brain stroke, and acute kidney injuries [21–23]. Nevertheless, few studies have analyzed the mechanism of ferroptosis in hepatic IRI. Yamada et al. recently reported that iron accumulation is a potential warning for IRI after liver transplantation [24]. Recent studies have suggested that HUWE1 is a potential protective factor that suppresses ferroptosis in liver damage caused by IRI or CCl₄ [25]. Notably, macrophage extracellular trap (METs) inhibition was reported to reduce ferroptosis in patients with hepatic IRI [26]. Therefore, blocking ferroptosis may be a potential therapeutic target for liver IRI.

DMF is a therapeutic agent for relapsing-remitting multiple sclerosis and psoriasis [27]. Even though its process is not well known, succinate cysteine residues have been reported to be covalently modified by DMF [28]. DMF treatment in a multiple sclerosis mouse model exhibited cellular protective and antioxidative effects [29]. Furthermore, a previous study revealed that DMF treatment ameliorated liver IRI in rats; however, the study focused on apoptotic and inflammatory status, lacked *in vitro* experiments, and did not investigate the underlying molecular mechanisms [30]. DMF also inhibited ferroptosis through the NRF2 signaling pathway in a chronic cerebral hypoperfusion model and alcoholic liver disease model, showing a significant protective effect [12,13]. This study revealed a previously

unidentified anti-ferroptosis role of DMF in liver IRI. It is interesting to note that Schmitt et al found DMF could induce ferroptosis and show an antitumor effect in germinal center B cell (GCB)-like diffuse large B-cell lymphoma (DLBCL) [31]. Although they found high 5-lipoxygenase expression in GCB DLBCL was correlated with an increased sensitivity to DMF-induced ferroptosis, the exact molecular mechanism was still unclear. The obvious difference in metabolism between tumor cells and normal cells may also be one of the reasons. The molecular mechanisms between DMF and ferroptosis needs to be further explored.

However, this study has some limitations. Further exploration is needed as to how DMF affects ferroptosis. The application of DMF on the protective effect of IRI induced liver damage has achieved good results, but efforts are still needed to explore the efficacy of DMF in the management of patients with liver transplantation and translate these experimental results into clinical applications.

One of the leading reasons for early organ dysfunction and failure after liver transplantation is IRI, an aseptic inflammatory response triggered by innate immunity [2]. DMF mediates its anti-inflammatory effects by downregulating aerobic glycolysis in activated myeloid and lymphoid cells [10]. Therefore, DMF may also improve IRI by modulating immunity. In addition, the shortage of donor liver tissues is a significant problem. Obesity and nonalcoholic fatty liver disease are becoming more common [16], the number of fatty donor livers available for transplantation is also increasing; however, fatty liver is more sensitive to IRI and is associated with a higher risk of early postoperative organ dysfunction or non-function [32]. Therefore, further studies should explore whether DMF can alleviate IRI in the fatty liver, which may help expand the donor pool.

The present study is the first to show that DMF reduces liver IRI via modulating ferroptosis via the NRF2/SLC7A11/HO-1 pathway, thereby providing a novel therapeutic strategy for IRI.

Disclosure statement

No potential conflict of interest was reported by the author(s).

Funding

The work was supported by the National Natural Science Foundation of China [82270681]; National Natural Science Foundation of China [81773172]

Data availability statement

The authors confirm that the data supporting the findings of this study are available within the article.

References

- [1] Saidi RF, Kenari SK. Liver ischemia/reperfusion injury: an overview. *J Invest Surg.* **2014**;27(6):366–379. Epub 2014/07/25PubMed PMID: 25058854.
- [2] Hirao H, Nakamura K, Kupiec-Weglinski JW. Liver ischaemia-reperfusion injury: a new understanding of the role of innate immunity. *Nat Rev Gastroenterol Hepatol.* **2022**;19(4):239–256. Epub 2021/11/28PubMed PMID: 34837066.
- [3] Gammella E, Recalcati S, Cairo G. Dual role of ROS as signal and stress agents: iron tips the balance in favor of toxic effects. *Oxid Med Cell Longev.* **2016**;2016:8629024. Epub 2016/03/24PubMed PMID: 27006749; PubMed Central PMCID: PMC4783558.
- [4] Jiang X, Stockwell BR, Conrad M. Ferroptosis: mechanisms, biology and role in disease. *Nat Rev Mol Cell Biol.* **2021**;22(4):266–282. Epub 2021/01/27PubMed PMID: 33495651; PubMed Central PMCID: PMC8142022.
- [5] Li J, Cao F, Yin HL, et al. Ferroptosis: past, present and future. *Cell Death Dis.* **2020**;11(2):88. Epub 2020/02/06PubMed PMID: 32015325; PubMed Central PMCID: PMC6997353.
- [6] Fang X, Wang H, Han D, et al. Ferroptosis as a target for protection against cardiomyopathy. *Proc Natl Acad Sci U S A.* **2019**;116(7):2672–2680. Epub 2019/01/30PubMed PMID: 30692261; PubMed Central PMCID: PMC6377499.
- [7] Lee H, Zandkarimi F, Zhang Y, et al. Energy-stress-mediated AMPK activation inhibits ferroptosis. *Nat Cell Biol.* **2020**;22(2):225–234. Epub 2020/02/08PubMed PMID: 32029897; PubMed Central PMCID: PMC67008777.
- [8] Li Y, Cao Y, Xiao J, et al. Inhibitor of apoptosis-stimulating protein of p53 inhibits ferroptosis and alleviates intestinal ischemia/reperfusion-induced acute lung injury. *Cell Death Differ.* **2020**;27(9):2635–2650. Epub 2020/03/24PubMed PMID: 32203170; PubMed Central PMCID: PMC7429834.
- [9] Sagasser J, Ma BN, Baecker D, et al. A new approach in cancer treatment: discovery of chlorido[N,N'-disalicylidene-1,2-phenylenediamine]iron(iii) complexes as ferroptosis inducers. *J Med Chem.* **2019**;62(17):8053–8061. Epub 2019/08/02PubMed PMID: 31369259.
- [10] Kornberg MD, Bhargava P, Kim PM, et al. Dimethyl fumarate targets GAPDH and aerobic glycolysis to modulate immunity. *Science.* **2018**;360(6387):449–453. Epub 2018/03/31PubMed PMID: 29599194; PubMed Central PMCID: PMC5924419.
- [11] Hu X, Li C, Wang Q, et al. Dimethyl fumarate ameliorates doxorubicin-induced cardiotoxicity by activating the Nrf2 pathway. *Front Pharmacol.* **2022**;13:872057. Epub 2022/05/14PubMed PMID: 35559248; PubMed Central PMCID: PMC9089305.
- [12] Yan N, Xu Z, Qu C, et al. Dimethyl fumarate improves cognitive deficits in chronic cerebral hypoperfusion rats by alleviating inflammation, oxidative stress, and ferroptosis via NRF2/ARE/NF- κ B signal pathway. *Int Immunopharmacol.* **2021**;98:107844. Epub 2021/06/22PubMed PMID: 34153667.
- [13] Zhang Y, Zhao S, Fu Y, et al. Computational repositioning of dimethyl fumarate for treating alcoholic liver disease. *Cell Death Dis.* **2020**;11(8):641. Epub 2020/08/20PubMed PMID: 32811823; PubMed Central PMCID: PMC7434920.
- [14] Yang Y, Cai F, Zhou N, et al. Dimethyl fumarate prevents ferroptosis to attenuate acute kidney injury by acting on NRF2. *Clin Transl Med.* **2021**;11(4):e382. Epub 2021/05/02PubMed PMID: 33931960; PubMed Central PMCID: PMC8087913.
- [15] Qiu YB, Wan BB, Liu G, et al. Nrf2 protects against seawater drowning-induced acute lung injury via inhibiting ferroptosis. *Respir Res.* **2020**;21(1):232. Epub 2020/09/11PubMed PMID: 32907551; PubMed Central PMCID: PMC7488337.
- [16] Younossi Z, Tacke F, Arrese M, et al. Global perspectives on nonalcoholic fatty liver disease and non-alcoholic steatohepatitis. *Hepatology.* **2019**;69(6):2672–2682. Epub 2018/09/05PubMed PMID: 30179269.
- [17] Koppula P, Zhuang L, Gan B. Cystine transporter SLC7A11/xCT in cancer: ferroptosis, nutrient dependency, and cancer therapy. *Protein Cell.* **2021**;12(8):599–620. Epub 2020/10/02PubMed PMID: 33000412; PubMed Central PMCID: PMC8310547.
- [18] Dong H, Qiang Z, Chai D, et al. Nrf2 inhibits ferroptosis and protects against acute lung injury due to intestinal ischemia reperfusion via regulating SLC7A11 and HO-1. *Aging (Albany NY).* **2020**;12(13):12943–12959. Epub 2020/07/01PubMed PMID: 32601262; PubMed Central PMCID: PMC7377827.
- [19] Liu H, Dong J, Song S, et al. Spermidine ameliorates liver ischaemia-reperfusion injury through the regulation of autophagy by the AMPK-mTOR-ULK1 signalling pathway. *Biochem Biophys Res Commun.* **2019**;519(2):227–233. Epub 2019/09/09PubMed PMID: 31493865.

- [20] Suzuki S, Toledo-Pereyra LH, Rodriguez FJ. Neutrophil infiltration as an important factor in liver ischemia and reperfusion injury. modulating effects of FK506 and cyclosporine. *Transplantation*. 1993;55(6):1265–1272. Epub 1993/06/01PubMed PMID: 7685932.
- [21] Gao M, Monian P, Quadri N, et al. Glutaminolysis and transferrin regulate ferroptosis. *Mol Cell*. 2015;59(2):298–308. Epub 2015/07/15PubMed PMID: 26166707; PubMed Central PMCID: PMC4506736.
- [22] Tuo QZ, Lei P, Jackman KA, et al. Tau-mediated iron export prevents ferroptotic damage after ischemic stroke. *Mol Psychiatry*. 2017;22(11):1520–1530. Epub 2017/09/09PubMed PMID: 28886009.
- [23] Friedmann Angeli JP, Schneider M, Proneth B, et al. Inactivation of the ferroptosis regulator Gpx4 triggers acute renal failure in mice. *Nat Cell Biol*. 2014;16(12):1180–1191. Epub 2014/11/18PubMed PMID: 25402683; PubMed Central PMCID: PMC4894846.
- [24] Yamada N, Karasawa T, Wakiya T, et al. Iron overload as a risk factor for hepatic ischemia-reperfusion injury in liver transplantation: potential role of ferroptosis. *Am J Transplant*. 2020;20(6):1606–1618. Epub 2020/01/08PubMed PMID: 31909544.
- [25] Wu Y, Jiao H, Yue Y, et al. Ubiquitin ligase E3 HUWE1/MULE targets transferrin receptor for degradation and suppresses ferroptosis in acute liver injury. *Cell Death Differ*. 2022;29(9):1705–1718. Epub 2022/03/10PubMed PMID: 35260822. DOI:
- [26] Wu S, Yang J, Sun G, et al. Macrophage extracellular traps aggravate iron overload-related liver ischaemia/reperfusion injury. *Br J Pharmacol*. 2021;178(18):3783–3796. Epub 2021/05/08PubMed PMID: 33959955.
- [27] Linker RA, Haghikia A. Dimethyl fumarate in multiple sclerosis: latest developments, evidence and place in therapy. *Ther Adv Chronic Dis*. 2016;7(4):198–207. Epub 2016/07/20PubMed PMID: 27433310; PubMed Central PMCID: PMC4935836.
- [28] Linker RA, Lee DH, Ryan S, et al. Fumaric acid esters exert neuroprotective effects in neuroinflammation via activation of the Nrf2 antioxidant pathway. *Brain*. 2011;134(Pt 3):678–692. Epub 2011/03/01PubMed PMID: 21354971.
- [29] Schulze-Topphoff U, Varrin-Doyer M, Pekarek K, et al. Dimethyl fumarate treatment induces adaptive and innate immune modulation independent of Nrf2. *Proc Natl Acad Sci U S A*. 2016;113(17):4777–4782. Epub 2016/04/15PubMed PMID: 27078105; PubMed Central PMCID: PMC4855599.
- [30] Takasu C, Vaziri ND, Li S, et al. Treatment with dimethyl fumarate ameliorates liver ischemia/reperfusion injury. *World J Gastroenterol*. 2017;23(25):4508–4516. Epub 2017/07/26PubMed PMID: 28740339; PubMed Central PMCID: PMC485504366.
- [31] Schmitt A, Xu W, Bucher P, et al. Dimethyl fumarate induces ferroptosis and impairs NF- κ B/STAT3 signaling in DLBCL. *Blood*. 2021;138(10):871–884. Epub 2021/04/21PubMed PMID: 33876201. DOI:
- [32] Chu MJ, Dare AJ, Phillips AR, et al. Donor hepatic steatosis and outcome after liver transplantation: a systematic review. *J Gastrointest Surg*. 2015;19(9):1713–1724. Epub 2015/04/29PubMed PMID: 25917535.